Available online at www.sciencedirect.com
SCIENCE DIRECT®
Inorganica Chimica Acta 359 (2006) 2210–2225
Inorganica Chimica Acta
www.elsevier.com/locate/ica

The kinetics and stereochemistry of base hydrolysis of the seven isomers of $[Co(dien)(ampy)Cl]^{2+}$ and $[Co(dien)(ibn)Cl]^{2+}$

Tao Zhu [a], W. Gregory Jackson [b,*], David C.R. Hockless [c], Anthony C. Willis [c]

[a] *Institute of Applied Chemistry, Guizhou University, Guiyang 550025, China*
[b] *School of Chemistry, University College, University of New South Wales, Australian Defence Force Academy, Northcott Drive, Canberra, ACT 2600, Australia*
[c] *Research School of Chemistry, Australian National University, Canberra, ACT 0200, Australia*

Received 13 November 2005; accepted 28 November 2005
Available online 15 March 2006

Abstract

The kinetics and stereochemistry for the base catalysed substitution reactions of all seven isomers (4 *mer* and 3 *fac*) of both $[Co(dien)(ibn)Cl]^{2+}$ and $[Co(dien)(ampy)Cl]^{2+}$ have been studied in detail, for water and azide ion as entering groups. The stereochemistry for the azide ion anation of some of the $[Co(dien)(diamine)OH]^{2+}$ species have also been investigated. The *mer* isomers are of comparable reactivity and amongst the fastest reacting pentaaminechlorocobalt(III) complexes known. They are also much faster to hydrolyse than the *fac* species. In both the ibn and ampy systems, a common product stereochemistry is observed for the four reactant *mer* isomers (the product is a mixture of all four *mer* configurations), for both azide ion and water as nucleophiles, but not for the three *fac* reactants (H_2O as nucleophile). The kinetic and equilibrium distributions are quite different. For the *mer* isomer reactions, a common trigonal bipyramidal five-coordinate intermediate deprotonated at the *sec*-NH of the dien is overwhelmingly implicated. The substitution mechanisms are argued in detail. Other data reported include isomerisation rates and equilibrium distributions for some *mer*-hydroxo and a *mer*-aqua complex of exceptional reactivity, equilibrium distributions for the *mer*-phosphato complexes in the ampy system under different pH conditions, the crystal structure for the isolated m1-$[Co(dien)(ampy)OP(OH)_3]Cl_3 \cdot 2H_2O$ species, and a rationale for its predominance at neutral pH based on internal H-bonding.

Keywords: Base hydrolysis; Phosphoric acid complex; Pentacoordinate intermediate; Diethylenetriamine; Aminomethylpyridine; Isobutylenediamine; X-ray structure

1. Introduction

The structurally related $[Co(dien)(ibn)Cl]^{2+}$ and $[Co(dien)(ampy)Cl]^{2+}$ systems are two for which all seven geometric isomers are known and which have been fully characterised by 2D NMR techniques [1,2], and single-crystal X-ray studies [3,4].

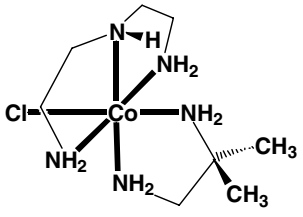

$[Co(dien)(ibn)Cl]^{2+}$

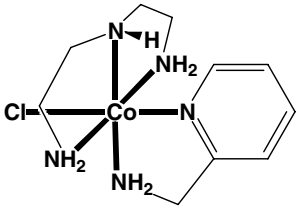

$[Co(dien)(ampy)Cl]^{2+}$

The isomers are shown (Fig. 1) for the ampy system, and a corresponding set exists for the ibn system.

* Corresponding author. Tel.: +61 2 62688078; fax: +61 2 62688090/8017.
E-mail address: wgj@adfa.edu.au (W.G. Jackson).

0020-1693/$ - see front matter © 2006 Elsevier B.V. All rights reserved.
doi:10.1016/j.ica.2005.11.050

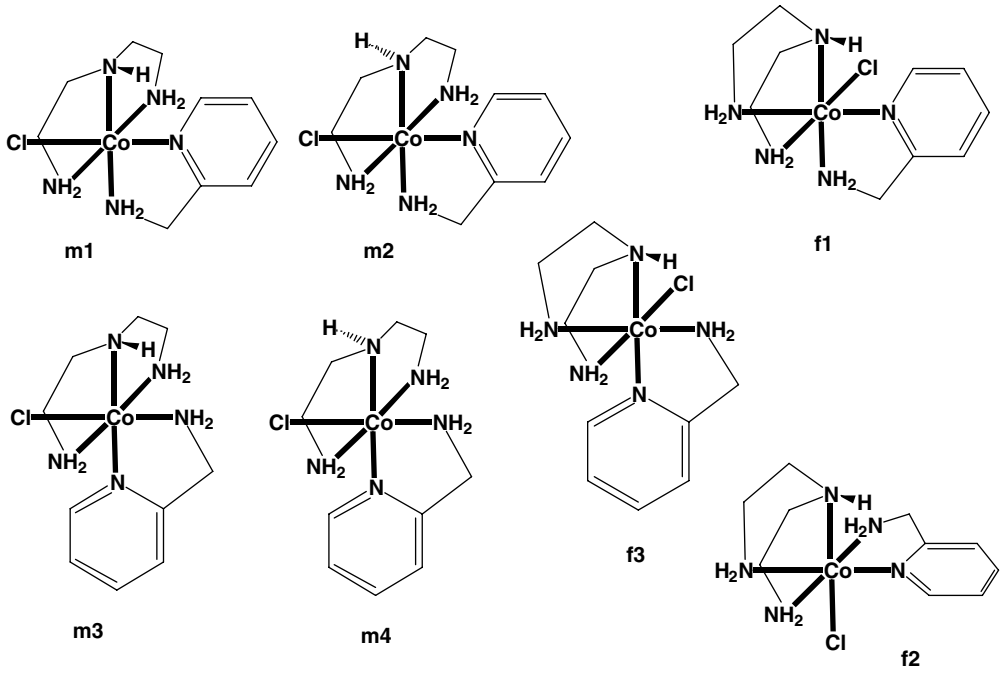

Fig. 1. The seven geometric isomers of $[Co(dien)(ampy)Cl]^{2+}$.

These systems were originally designed to probe the subtler aspects [5] of the base hydrolysis mechanism. While ibn and ampy are stereochemically similar, there are some significant differences. First, the two 'ends' of the diamine are different in the sense that in ampy a terminal NH_2 is blocked by a pyridyl, which removes a potential deprotonation site for base hydrolysis. If this were the reactive site for base catalysed hydrolysis, then two of the four *mer* isomers would be much more reactive than the other two, if, for example, deprotonation at $-NH_2$ on the bidentate ligand *trans* (or *cis*) to Cl^- was generally preferred. Further, the ampy chelate ring is flatter than for ibn. Finally, the stereochemistry of the pyridyl substituted material is such that the two possible paths for the re-entering group Y in the favoured trigonal bipyramidal intermediate in this reaction are very much different (Fig. 2) compared to ibn (the *cis* or *trans* isomers are defined by the position of the pyridyl or $C(CH_3)_2$ group relative to the *sec*-NH).

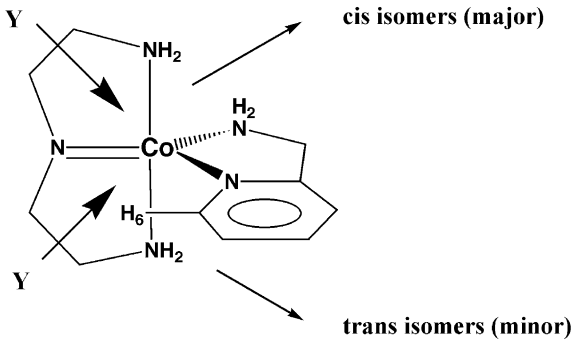

Fig. 2. Decay paths for the favoured five-coordinate trigonal bipyramidal intermediate in the *mer*-$[Co(dien)(ampy)X]^{n+}$ system.

The H6 proton blocks one of the pathways for the re-entering group, leading to a *cis* isomer preference. On the other hand, from the viewpoint of relative stability, the *trans* isomer might be expected to be the major product because there is less steric interaction between H6 and the *sec*-NH centre. Thus, the *cis* isomer(s) would be predicted to be dominant at the beginning of base hydrolysis (kinetically preferred), with subsequent rearrangement to the more stable *trans* isomers. Finally, if each of the four *mer* isomers gave the same kinetic product distribution, this would be additional and strong evidence for the suggested intermediate type, which is the only one for which the *cis*/*trans* and *syn*/*anti* distinctions are removed.

Herein, we report a comprehensive study of the base catalysed substitution reactions for the $[Co(dien)(ibn)Cl]^{2+}$ and $[Co(dien)(ampy)Cl]^{2+}$ systems, including water and azide capture and isomerization reactions of intermediate hydroxo and azido products.

2. Experimental

All chemicals were analytical or an equivalent grade. ^{13}C and ^{1}H NMR spectra were recorded on a Varian XL 300 MHz instrument at 20 °C. Solvents used were D_2O with dioxane as an internal reference (^{13}C, δ 69.27; ^{1}H, δ 3.75 ppm relative to DSS), and Me_2SO-d_6 with the central peak of the CD_3 septet as the reference (^{13}C, δ 39.37; ^{1}H, δ 2.50 ppm relative to $SiMe_4$). UV–Vis absorption spectra (600–300 nm) and absorbance–time traces were obtained with use of a HP 8452 A Diode-Array spectrophotometer thermostated to 25.0 ± 0.1 °C, with Specfit® software to extract and analyse the kinetic data. The data were

routinely checked to ensure absorbances in the wavelength range chosen for analysis did not exceed 1.5, and that the data covered at least 2 $t_{1/2}$ of reaction (more usually 3–4 $t_{1/2}$). All kinetic runs were performed in triplicate, using [Co] in the range 0.001–0.01 M to achieve the desired absorbance change.

2.1. Buffer solutions

The buffer solutions were made up with TES (0.200 M) (TES = *N*-[tris(hydroxymethyl)]-2-aminoethanesulfonic acid), partly neutralised by addition of Convol NaOH (1.000 M) and of total ionic strength 1.0 M (NaCl); the ratio of [TES]/[TES$^-$] ranged from 9/1 to 1/9 to cover about 2 pH units. NaCl was chosen as the supporting electrolyte in place of the more usual $NaClO_4$, one for reasons of complex solubility, and two, because Cl^- is a poorer competitor than ClO_4^- in base catalysed substitution reactions [6,7]. No problems of reversibility of the hydrolysis reactions were observed for 1 M Cl^-. p[H] determinations were made as described previously [8].

2.2. Synthesis, separation and characterisation of the $[Co(dien)(ibn)X]^{2+}$ and $[Co(dien)(ampy)X]^{2+}$ (X = Cl, OH_2 and N_3) isomers

The chloro and azido complexes were completely described in previous publications [1,2]. The methods used to synthesise specific stereoisomers of the aqua species depended on the particular isomer required.

Method 1: A solution of $Hg(trif)_2$ (5 mL, ca. 1.5 M; from yellow HgO in excess aqueous CF_3SO_3H) was added to one of the [Co(dien)(diamine)Cl]Cl_2 isomers (0.5 g) dissolved in water (1 mL). The solution was left at ambient temperature until the colour of the solution changed to orange-yellow, then cooled in an ice-bath. Concentrated HCl was added just until the precipitated $HgCl_2$ redissolved, then poured into 500 mL of acetone. The chloride salt of the aqua species was collected by filtration, and recrystallised from water/HCl by careful dilution with acetone. This method proved suitable for the facial (f1, f2, f3) and *syn–mer* (m2, m4) isomers.

Method 2: This method was convenient for the synthesis of chloride free *mer*-aqua species. The pure perchlorate salt of the appropriate *mer*-azido isomer (0.10 g) was dissolved or suspended in 3 M $HClO_4$ or triflic acid (5 mL), cooled in an ice-bath, and sodium nitrite (0.050 g) was added to the solution in small proportions. After the evolution of gas had ceased, the solution was degassed (ultrasonic bath) and then loaded on to a Biorex MSZ 50 column (Na^+ form) and then washed with water. Elution with 0.2 M $NaClO_4$/0.05 M $HClO_4$ yielded an orange band. The eluate was reduced in vacuo at <35 °C to a small volume whereupon the perchlorate salt crystallised. The crystals were collected, washed with isopropanol and ether, and air dried.

2.3. Product distributions

A specific isomer of [Co(dien)(ibn)X]Cl_2 or [Co(dien)(ampy)X]Cl_2 (X = Cl, OH_2 or N_3; ca. 50 mg) was dissolved in D_2O (0.2 g), and an equal volume of 1.0 M NaOD (Pipetman®) was added while stirring rapidly (0 or 20 °C). The reactions were quenched with cold $HClO_4$ (70%; 0.15 mL). For the reactions at 20 °C, a series of experiments were performed, at specific reaction times (0–60 s), and the product distribution data in all cases were evaluated by ^{13}C NMR spectroscopy. A separate experiment was performed for each reaction time, and involved a large number of determinations (each in triplicate). Because there were four isomeric products, in situ NMR analysis (±5% for each component) was superior to chromatographic separation and analysis for the individual species (of the aqua ions, or chloro ions reformed by heating in HCl (shown to be retentive)). In situ spectrophotometric analysis is quite inaccurate where there are four components and the UV–Vis spectra are quite similar.

The product distributions for the base hydrolysis of the *fac*-chloro and *mer*-azido species were carried out similarly (20 °C), as were the experiments on the four *mer*-chloro and aqua ions reacted in unbuffered 1 M NaN_3 (20 °C). The NMR tubes from all experiments were retained (in the dark) for periods sufficient to observe the equilibrium distributions.

2.4. X-ray structural determination

X-ray diffraction data were collected on an orange crystal of [Co(dien)(ampy)$OP(OH)_3$]$Cl_3 \cdot 2H_2O$ using a Rigaku AFC-6S diffractometer.

The structure was solved by direct methods (SIR-92) [9] and refined using the teXsan computer software package [10]. Difference electron density maps revealed H atoms

Table 1
Crystal data for *mer–anti*-[Co(dien)(ampy)$OP(OH)_3$]$Cl_3 \cdot 2H_2O$

Formula	$C_{10}H_{24}Cl_3CoN_5O_4P \cdot 2H_2O$
M	510.63
Crystal system	triclinic
Space group	$P\bar{1}$
a (Å)	8.061(3)
b (Å)	10.405(2)
c (Å)	12.739(2)
α (°)	95.48(2)
β (°)	93.90(2)
γ (°)	100.01(2)
V (Å^3)	1043.5(5)
Z	2
T (K)	296.2
λ(Mo Kα) (Å)	0.71073
D_{calc} (g cm^{-3})	1.625
μ (cm^{-1})	13.18
Number of observed/unique data	3032 ($I > 3\sigma(I)$)
Number of refined parameters	257
R	0.030
R_w	0.039
S	1.70

on O(2), O(3) and O(4) and on the O atoms of the water molecules. These H atoms were included in the structure and their coordinates were refined. Restraints were imposed on bond distances and angles for the water molecules. H atoms bonded to N and C atoms were included at calculated position and were not refined. Crystal and refinement details are given in Table 1.

3. Results and discussion

3.1. Kinetics of base hydrolysis of the $[Co(dien)(ibn)Cl]^{2+}$ isomers

Preliminary plots of k_{obsd} versus $[OH^-]$ (0–5×10^{-6} M) for the four *mer*-isomers were markedly curved (not shown), and each apparently follows an equation of the form $k_{obsd} = k_1[OH^-]/(1 + K[OH^-])$. The origin of the curvature for the *mer* plots was initially unclear. In this $[OH^-]$ range, net deprotonation, which would accommodate the convex curvature, is not expected. A closer examination of the spectral data where there were maximal spectral changes (300–360 nm) revealed clean isosbestic points and uniphasic behaviour (to ca. 3 $t_{1/2}$) for the first few buffers at the lower pH end, consistent with simple $[Co(dien)(ibn)Cl]^{2+}$ hydrolysis to $[Co(dien)(ibn)OH]^{2+}$. The specific rates were essentially linear in $[OH^-]$ in this region. Yet around pH 7, biphasic kinetics were clearly evident; a single exponential did not fit the data well, and there were no isosbestic points (''shifting isosbestics'' are observed). A reasonable fit to the data could be obtained using just the first two half lives of absorbance–time traces, or fitting the data to a consecutive first-order reaction scheme. It is noted, however, that extracting reliable rate constants for consecutive reactions where the component rate parameters are within a factor of two is intrinsically difficult [11,12]. Using Specfit® the slow-fast ambiguity was resolved by calculating the spectra for the first formed species. Only one scheme (fast-slow) yielded a reasonable spectrum, the other (slow-fast) gave a nonsensical one (negative absorbances).

The rate constant for the second step(s) (isomerisation of the *m*-OH^{2+} species, studied independently – see ahead), while not accurately defined in these experiments, proved to be approximately constant (2×10^{-3} s^{-1}, 25 °C), except at lower pH where its value was diminished. This observation is consistent with the expected pH independence of the isomerisation rates for *m*-OH^{2+}, at pH values above the pK_a of its aqua conjugate acid (pK_a ca. 6). The reduction in rate at ca. pH 6 is therefore consistent with its partial conversion into the relatively unreactive aqua complex. The subsequent isomerisation process is not single phasic – all four *mer* isomers are involved, since base hydrolysis of any of the *mer*-chloro ions initially produces all four *mer*-hydroxo ions.

At the highest pH studied, the kinetics were again uniphasic, and first order. We discovered, however, that the measured rate was that for the second step, and not for the base hydrolysis of the chloro complex. The latter was simply too fast to measure under the conditions. Thus, the curvature first seen at higher $[OH^-]$ was an artefact – the measured rate constants were not for the same process. Fig. 3 shows the rate plot for the correct data.

While the data are not especially accurate, the trends are clear. We do not regard the (small) intercepts, which are the k_s values, as particularly accurate.

This analysis emphasises how one can be easily misled when dealing with multi-isomer systems and where one needs to be aware of kinetic possibilities that can mask the real facts. As noted previously [13], the kinetic behaviour of all reactant and product isomers need be known to be confident that the intrusion of a 'missing' isomer has not skewed the analysis.

The kinetics for the *fac* isomers was not subject to the problems just outlined because the reactions are much slower and the subsequent (fast) mutarotation of *mer*-OH is easily separated out in the data analysis. Also, the products are largely the *fac*-OH species that are relatively unreactive ions. Plots of k_{obsd} versus $[OH^-]$ are linear (Fig. 4).

3.2. Kinetics of base hydrolysis of the $[Co(dien)(ampy)Cl]^{2+}$ isomers

Again the problem that arose with the *mer* isomer kinetics in the $[Co(dien)(ibn)Cl]^{2+}$ system was encountered. Biphasic kinetics were observed, arising from competitive rearrangement of the product hydroxo species. At higher pH, the rearrangement is the slower step, and the primary hydrolysis is too fast to determine accurately. To resolve the issue, the data were restricted to the lower pH region; plots of k_{obsd} versus $[OH^-]$ for the four *mer*-isomers are linear (Fig. 5). Plots of k_{obsd} versus $[OH^-]$ for the three facial isomers are also linear (Fig. 5).

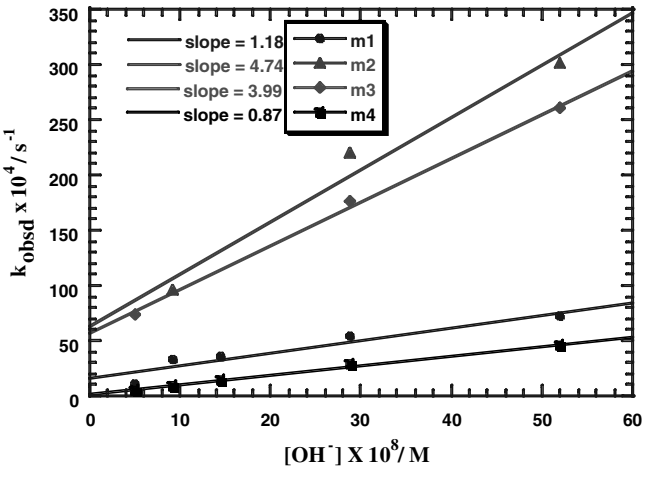

Fig. 3. Plot of observed rate constants vs. $[OH^-]$ for the base hydrolysis of the four *mer* isomers of $[Co(dien)(ibn)Cl]^{2+}$ in TES buffers ($I = 1$ M, NaCl) at 25 °C. The slopes are k_{OH} values (M^{-1} s^{-1}), the intercepts k_s values (s^{-1}).

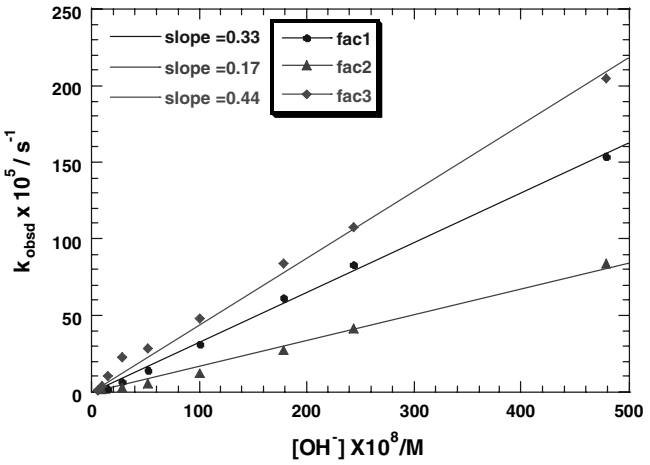

Fig. 4. Plot of observed rate constants vs. $[OH^-]$ for the base hydrolysis of the three *fac* isomers of $[Co(dien)(ibn)Cl]^{2+}$ in TES buffers ($I = 1$ M, NaCl) at 25 °C.

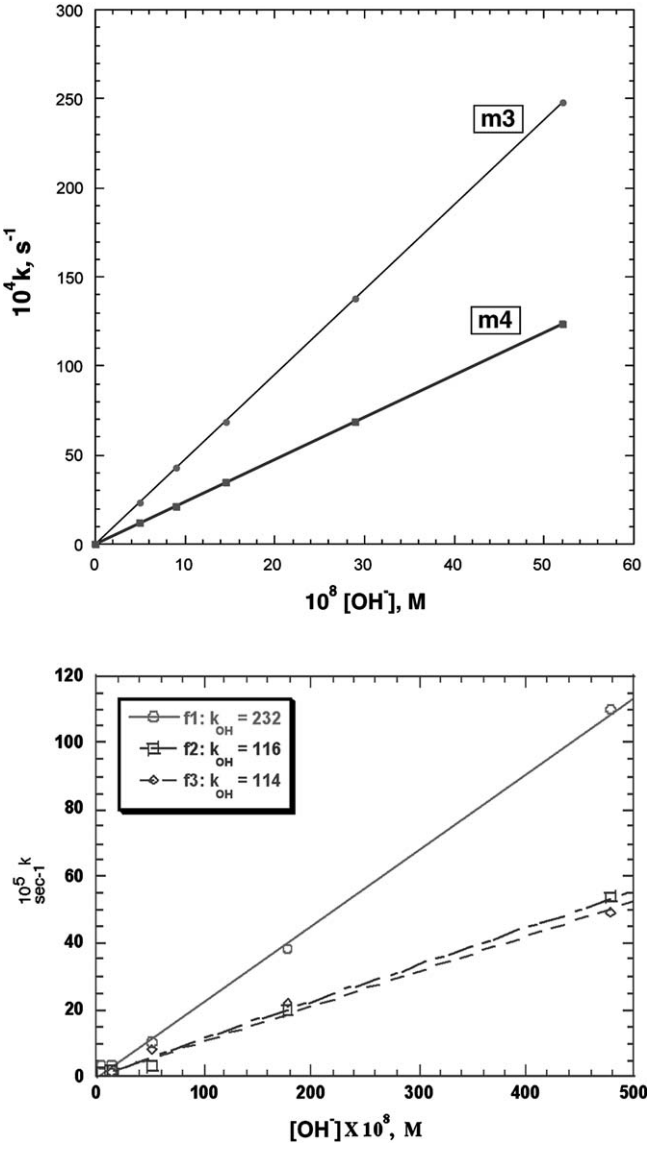

Fig. 5. Kinetic results for two of the four *mer* and the three facial isomers of $[Co(dien)(ampy)Cl]^{2+}$ in TES buffers ($I = 1$ M, NaCl) at 25 °C.

The hydrolysis rates for the m1 and m2 isomers were too fast to determine over the complete pH range shown; we measured the rates at two low $[OH^-]$ values, 9×10^{-8} and 1.45×10^{-7} M, and also in acid where the rates were immeasurable slow compared to very dilute $[OH^-]$. The average results were $k_{OH} = 8.9 \times 10^6$ for the m1 and 8.0×10^6 M^{-1} s^{-1} for the m2 form.

3.3. Reactivity comparisons

The rate data for the ibn, ampy and en systems are summarised in Table 2.

The *mer–cis* isomers in the ampy system are 5- to 10-fold more reactive than the *mer–trans* isomers, but this is not apparent for the corresponding ibn system. In the *cis* isomers there appears to be a steric interaction of the pyridyl of ampy with the *sec*-NH of dien, and movement to the preferred trigonal intermediate (vide infra) does alleviate this interaction, and this may reflected in the base hydrolysis rates to a mild extent. The *syn*/*anti* rate differences are also relatively small (up to a factor of 5), and inconsistent – the *syn* can be more or less reactive than the *anti* form [14]. The high reactivities of the ampy complexes are typical for *mer*-$[Co(dien)(diamine)Cl]^{2+}$ complexes [15–19]. Also, switching the ampy ligand to alternately block deprotonation sites *cis* and *trans* to Co–Cl, has no profound effect. This result is entirely consistent with the finding (ahead) that the effective deprotonation site is not on the diamine but rather on the dien triamine. The intercepts in the plots shown in Fig. 5, which reflect the 'acid' hydrolysis rates, i.e., the rates of aquation (k_s), are indistinguishable from zero; they are negligible compared to the rates for the base catalysed path.

There is a 1000-fold difference between the reactivity of the *mer* and facial isomers, for all these diamine systems [14,20–22]. The consistent difference indicates that for the *fac* isomers the effective deprotonation site also resides on the dien ligand, but clearly it is very much less effective.

3.4. Base catalysed substitution in $[Co(dien)(ibn)Cl]^{2+}$

At high $[OH^-]$ (0.5 M $NaOD/D_2O$), the hydrolysis of all of the isomers of $[Co(dien)(ibn)Cl]^{2+}$ is complete within

Table 2
Base hydrolysis rate data for the $[Co(dien)(diamine)Cl]^{2+}$ systems; $I = 1$ M NaCl, 25 °C (TES buffers)

Reactant isomer	k_{OH} (M^{-1} s^{-1})		
	ibn	ampy	en[a]
m1	11800	890000	7800
m2	47400	800000	10500
m3	40000	48000	7800
m4	8700	24000	10500
f1	330	230	27
f2	170	110	0.7
f3	440	110	27

[a] The m1 and m3 (*anti*) forms are not distinguished for symmetrical diamines such as en, nor are m2 and m4.

seconds. Control experiments were carried out on pure *mer*- and *fac*-hydroxo ions reacted under the same conditions, to ascertain the relative rates of subsequent isomerisation (vide infra). For the *mer*-chloro reactants, two sets of experiments were performed, one set at 0 °C (1 s quench), and another at ambient temperature, at intervals covering a complete reaction time of 60–80 s.

Table 3 shows the kinetic product distributions for the base hydrolysis of all isomers in each system (ibn, ampy, en).

Table 4 details the *cis*/*trans* and *syn*/*anti* product ratios for the *mer* isomers of $[Co(dien)(ibn)Cl]^{2+}$. There are no *fac*-OH products, but rather a mixture of the *m*-OH species. These are the kinetic distributions; the equilibrium values are quite different (Table 3). Further, subsequent isomerization of the first formed hydroxo ions is very much slower than base hydrolysis of the chloro substrates, at higher concentrations of OH^-. Further, in experiments where the base hydrolysis of a chloro isomer was acid quenched prior to completion, recovered reactant proved to be a single unchanged isomer. Since two of the four *mer*-OH products have their *sec*-NH centre inverted, it is clear that N-inversion occurs *during* the act of base hydrolysis, thus identifying the site of deprotonation. The second significant result is that, within experimental error (±5%), the product distributions are identical for each of the four *mer* substrates (Table 5). The clear implication is that a common reduced coordination number intermediate is involved, and the only conceivable structure common to all four *mer* substrates is the one shown (Fig. 6), in which the *cis*/*trans* and *syn*/*anti* distinctions are lost.

A species deprotonated at a site other than the *sec*-NH, for example, can give rise to only two products, not four,

Table 3
Steric course of base catalysed substitution for individual $[Co(dien)(diamine)Cl]^{2+}$ isomers

Ligand system	Reactant isomer[a,b]	Product distribution (%)						
		m1	m2	m3	m4	f1	f2	f3
ibn	m1	14	36	16	44	0	0	0
	m2	15	30	15	40	0	0	0
	m3	16	34	16	34	0	0	0
	m4	17	32	15	36	0	0	0
	f1	40	0	0	0	49	11	0
	f2	0	0	0	0	24	76	0
	f3			40			11	49
ampy	m1	71	0	23	6	0	0	0
	m2	80	0	14	6	0	0	0
	m3	79	0	17	4	0	0	0
	m4	77	0	17	8	0	0	0
	f1	8	0	0	0	80	12	0
	f2	0	0	0	0	67	33	0
	f3			12				88
en	m1/3[c]							
	m2/4[c]							
	f1/3[c]		50[c]			50[c]		
	f2[d]						60[c]	40[c]

[a] *mer* reactants, 0 °C.
[b] *fac* reactants, 20 °C.
[c] m1 and m3 (*mer*–*anti*) isomers are not distinguished for the symmetrical bidentate en, nor are m2 and m4 (*mer*–*syn*), nor f1 and f3 (unsym-*fac*; π in the old nomenclature).
[d] sym-*fac* (ω in the old nomenclature).

Table 4
Kinetic product ratios for the base hydrolysis of $[Co(dien)(ibn)Cl]^{2+}$ at 0 °C

Product ratios:	*trans*/*cis*		*anti*/*syn*	
Precursor:	m3/m1	m4/m2	m1/m2	m3/m4
m1-Cl	1.1	1.4	0.4	0.4
m2-Cl	1.0	1.3	0.5	0.4
m3-Cl	1.0	1.0	0.5	0.5
m4-Cl	0.9	1.1	0.5	0.4

Table 5
Kinetic and equilibrium $[Co(dien)(diamine)N_3]^{2+}$ product distribution data for the base catalysed substitution of *mer*-$[Co(dien)(diamine)X]^{2+}$ (diamine = ibn, ampy, en) in unbuffered 1 M NaN_3, 20 °C

Diamine	Reactant	mer1 (%)	mer2 (%)	mer3 (%)	mer4 (%)	*syn* (%)	*cis* (%)
Kinetic							
ibn	mer1-Cl	22	27	19	33	60	49
	mer2-Cl	17	27	12	44	61	44
	mer3-Cl	16	27	15	32	59	43
	mer4-Cl	26	24	20	30	54	50
ampy	mer1-Cl	42	50	0	8	58	92
	mer2-Cl	45	47	0	8	55	92
	mer3-Cl	50	41	0	9	50	91
	mer4-Cl	50	40	0	10	50	90
en	mer1/3-Cl	45[a]	55[b]			55	
	mer2/4-Cl	45[a]	55[b]			55	
Equilibrium							
ibn	mer1-Cl	27	9	37	27	36	36
	mer2-Cl	29	8	39	26	34	37
	mer3-Cl	29	8	44	16	24	37
	mer4-Cl	21	3	61	15	18	24
ampy	mer1-Cl	81	5	0	14	19	86
	mer2-Cl	83	3	0	14	17	86
	mer3-Cl	82	4	0	14	18	86
	mer4-Cl	82	5	0	14	19	87
	mer3-OH	82	5	0	13	18	87
en	*mer*-Cl	87[a]	13[b]			13	

[a] *anti* isomer.
[b] *syn* isomer.

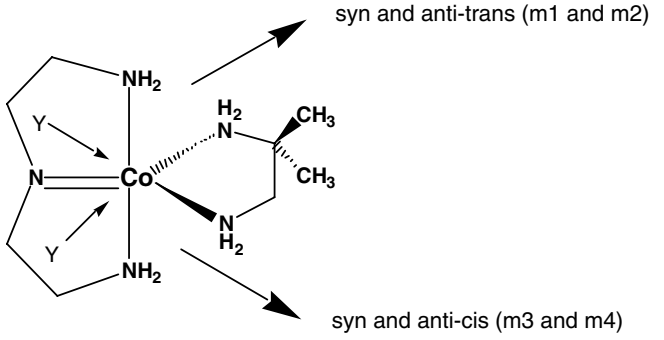

Fig. 6. The proposed pentacoordinate intermediate for the base catalysed substitution of *mer*-$[Co(dien)(ibn)X]^{n+}$ complexes.

and the *sec*-NH configuration would be retained, contrary to observation.

In 1 M NaN_3, base hydrolysis of the *mer*-chloro complexes is accompanied by the production of not only four *mer*-hydroxo ions but also some (ca. 30%) azido complexes, also as a mixture of four *mer* isomeric forms (Table 5). In the pH region studied (ca. 8–9), the azido ions are considerably more robust than their corresponding hydroxo ions, and the latter could be observed to anate and isomerise to yield ultimately all azido complex, without affecting the kinetic distribution of *mer*-azido isomers. No attempt was made to separate out the contributions from these initial and secondary reactions, both of which are must faster than the ultimate equilibration via isomerization and N-inversion in the azido products. Also, the equilibrium azido complex values are quite different to the initial isomer proportions, as they are also for the hydroxo distributions (Table 6).

The observed azido distribution is both a kinetic one and a composite, representing the distributions for hydrolysis of the chloro ion and the subsequent azide anation of first formed hydroxo ions. However, the product distributions derived from all four *mer*-Cl isomers, and the hydroxo ions, are identical, reinforcing the concept of a common pentacoordinate intermediate in which the *cis*/*trans* and *syn*/*anti* distinctions are lost (Fig. 6). It is noted that attack in the trigonal plane is different for the two entry sites, and the product *cis*/*trans* ratios are not 1:1, and they also depend upon the nucleophile (Table 6). However, $C(CH_3)_2$ versus CH_2 in the backbone of the chelate does not provide a large difference, with the kinetically preferred total *cis* product being close to 50% for both water and azide as nucleophiles (for attack from the side away from the gem dimethyl group). At equilibrium, there is a tendency to more *trans*, for both N_3^- and OH^- as ligands, but it is not pronounced.

It is important to recall [23] that the formation of the pentacoordinate intermediate via deprotonation at the *sec*-NH followed by loss of the leaving group will be mirrored in the decay path to products, i.e., attack by the entering group (H_2O or N_3^-) followed by reprotonation. Given this sequence of events, it can be seen that both the *cis*/*trans* and *syn*/*anti* kinetic distributions are determined in the first of these two product determining steps. The final reprotonation merely locks in the now reformed pyramidal configuration at the *sec*-N centre. Thus, the first step of nucleophilic attack in the trigonal plane might be anticipated to be fairly indiscriminate given the ca. 120° angle as opposed to the 90° angle of the octahedron. Indeed, this is the case for the *syn*/*anti* as well as the *cis*/*trans* distributions which are all close to 50:50. Contrast the equilibrium distributions where the *anti* forms are favoured for the octahedral ions.

In strong OH^- the azido isomers completely base hydrolyse, and we have measured both the kinetic and

Table 6
Summary of base hydrolysis kinetic[c] and equilibrium[d] product distribution data for *mer*-$[Co(dien)(diamine)X]^{2+}$ (diamine = ibn, ampy, en)

Diamine	Reactant	Nucleophile	mer1 (%)	mer2 (%)	mer3 (%)	mer4 (%)	*syn* (%)	*cis* (%)
Kinetic								
ibn	*mer*-Cl	H_2O	15.5	33	15.5	36	69	48.5
	mer-N_3	H_2O[e]	16	29	20	35	64	45
	mer-Cl	N_3^-	20	27	17	36	62	46
ampy	*mer*-Cl	H_2O	76	0	18	6	6	76
	mer-Cl	N_3^-	46.5	44.5	0	9	53.5	91
	mer-OH	N_3^-	45	47	0	8	55	92
en	*mer*-Cl	H_2O	46[a,b]	54[a,b]			54	
	mer-Cl	N_3^-	55[a,b]	45[a,b]			45	
	mer-OH	N_3^-	58[a,b]	42[a,b]			42	
Equilibrium								
ibn	*mer*-Cl	H_2O	29	3	59	9	12	32
	mer-N_3	H_2O	35	6	49	10	16	41
	mer-Cl	N_3^-	26	7	46	21	28	33
ampy	*mer*-Cl	H_2O	8	0	80.5	11.5	11.5	8
	mer-Cl	N_3^-	82	4	0	14	18	86
	mer-OH	N_3^-	82	5	0	13	18	87
en	*mer*-Cl	H_2O	87[a,b]	13[a,b]			13	
	mer-OH	H_2O	87[a,b]	13[a,b]			13	
	mer-Cl	N_3^-	89[a,b]	11[a,b]			11	
	mer-OH	N_3^-	89[a,b]	11[a,b]			11	

[a] The m1 and m3 (*anti*) isomers are not distinguished for the symmetrical diamine en, nor are the m2 and m4 (*syn*) isomers.
[b] Ref. [25].
[c] Reaction time 40 min, 0 °C.
[d] Reaction time 2 days, 20 °C.
[e] 20 °C.

equilibrium distributions for the hydroxo products, as described for the chloro reactants. The results are again identical within experimental error (±5%), despite the big difference in the reactivity of the chloro and azido complexes (Table 6). In the $[Co(NH_3)_5X]^{n+}$ system, k_{OH} for $X = Cl^-$ is almost 800-fold greater [19] than that for $X = N_3^-$.

In summary, common kinetic distributions, independent of the starting *mer* geometry and also the leaving group (Cl^-, N_3^- or H_2O) argue for a common intermediate of the type shown (Fig. 6). The hydroxo ions in these reactive *mer* systems substitute via internal conjugate base process established previously for the dapo [24] and en [5] systems and involving a reactive substrate of the type shown, analogous to that derived from the chloro reactants (Fig. 7). Note that there is no requirement for the NH to be *syn* to the coordinated OH^- to get internal proton transfer here since proton transfer is not rate determining.

Finally, it should be noted that the *common* "equilibrium" distributions do not necessarily imply that the azido systems are at equilibrium (amongst the *mer* isomers), since a common result would flow from the common initial distributions, if the reaction times were the same (and they were). This aspect has been checked by remeasuring some of the systems at much longer reaction times. We found the same ratio for the four *mer* isomers, but together with some of the *fac* isomers. It is concluded that the equilibrium distributions shown in Tables 5 and 6 are correct.

3.5. Base catalysed substitution in $[Co(dien)(ampy)Cl]^{2+}$

It was anticipated that the major kinetically preferred products would be largely *cis* (m1 and/or m2), whereas the equilibrium distribution should be largely *trans*. This is borne out by the results (Tables 2 and 6) for water as the nucleophile, but not for azide which prefers to be *cis*

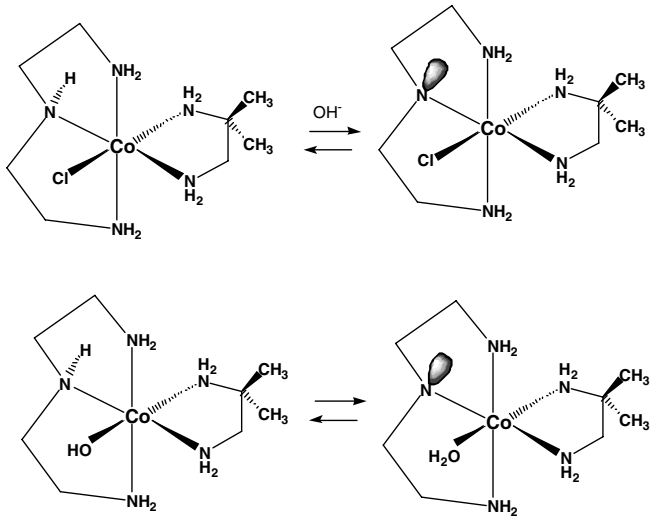

Fig. 7. The top diagram shows the normal deprotonation step in base catalysed hydrolysis, which requires external OH^- and gives rise to the usual second-order kinetics. The lower one shows the internal proton transfer for a hydroxo complex, requiring no external OH^-, but generating an identical reactive species, differing only in the leaving group.

even under equilibrium conditions (Table 6). Secondly, and the major point, the kinetic distributions are independent of source, again consistent with an intermediate which has lost not only Cl^- but also memory of its origin (*syn*/*anti* and *cis*/*trans*) (Fig. 8).

The common product distribution 77%, 0%, 17%, 6% (m1, 2, 3, 4) observed for the entry of water is quite different to the equilibrium distribution – 8%, 0%, 80%, 12%.

For the four *mer*-Cl isomers reacted in unbuffered NaN_3 (1 M, 20 °C), the corresponding *mer*-azido product distributions were 47, 44, 0, 9 and 82, 4, 0, 14, again independent of the starting geometry, but results different to water as a

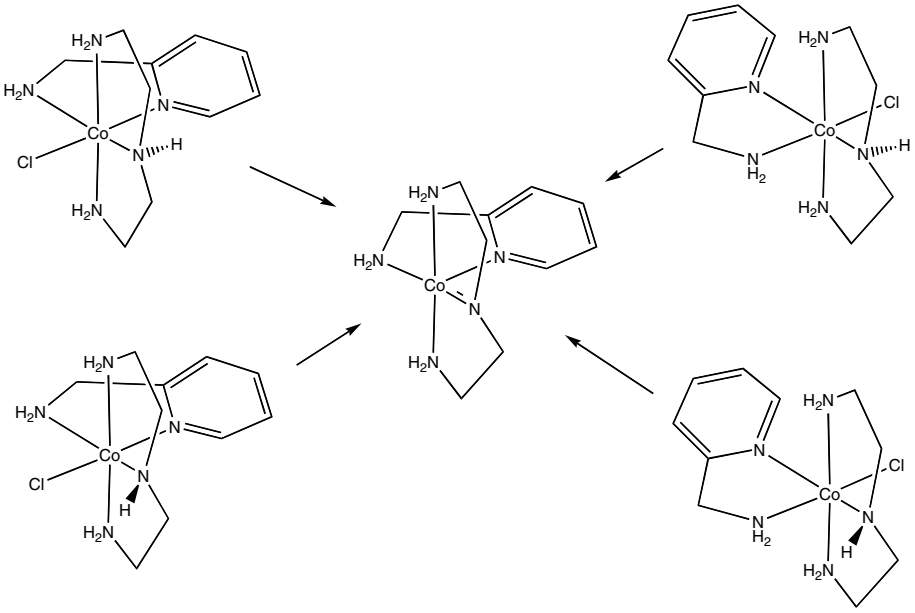

Fig. 8. The symmetrical π-bonded TBP intermediate derived from the four different *mer* substrates.

nucleophile. No *anti–mer–trans* isomer (m3) was observed initially or at equilibrium, whereas the m2 isomer, unobserved for water as a nucleophile, was now a major kinetic product. These features were exploited synthetically to prepare the putative m2-Cl and m4-Cl complexes.

Figs. 9 and 10 show the initial and final azido isomer distributions for three different *mer* reactants. The azido products are normalised to 100% to show the agreement between the initial and final values, and the same rates of decay, independent of source (Cl^- or OH^- as leaving group, m1 or m3 configuration). The decay of the starting material is also shown, to indicate the relative rates in the three systems, and to indicate the difficulty of accurately defining the product distributions under conditions where the substrate has not completely decayed before the products have started to rearrange.

The azido products at very early reaction times were quite dominant, with little competitive hydrolysis (based on analysis by NMR), indicating in crude terms the capture of >50% total azido product for 1 M N_3^- (and thus <50% hydroxo species). This level of anion competition is not inconsistent with studies for the simpler systems such as *mer*-$[Co(dien)(en)Cl]^{2+}$ where the actual competition values have been determined [25] and are of the order of 50% azide capture for 1 M NaN_3.

The most stable hydroxo complex is the m3 isomer, whereas for the azido species it is the m1 isomer; each of these has the favoured *anti*-NH form. These results show clearly that the nature of the sixth ligand X in *mer*-[Co(dien)-(ampy)X] can significantly affects the relative energies of the isomers. This has been already observed for the phosphate complexes (see 3.7 ahead) where we argue a special H-bonding effect for the m1 isomer, but it is clear that simply changing the ligand can change the preferred configuration. We can see no particular properties of bound hydroxide or azide ion that brings about these configurational preferences. Finally, it is noted that the preferred *sec*-NH configuration for the *trans* azido species is exclusively *endo* (m4). This is unusual and as yet is not understood.

3.5.1. Rearrangement of m2-$[Co(dien)(ampy)OH_2]^{3+}$ in aqueous acid

In the base hydrolysis studies, the m2-OH species (*syn*) was not observed, even under equilibrium conditions, although the expectation was the usual *syn* (*endo*) and *anti* (*exo*) isomers first-formed in comparable amounts. We have also found that the m2- (and m1-) chloro ions hydrolyse in acid remarkably quickly. We therefore suspected that the m2-OH ion is unusually labile, and isomerises to the more stable m1-form to escape detection (the amount of first-formed m1 isomer is anomalously high). This can occur via an internal conjugate base process [24], whereby N-inversion occurs via the hydroxo complex by transferring an NH proton to generate water as the leaving group (Fig. 7), or it can occur by direct N-inversion.

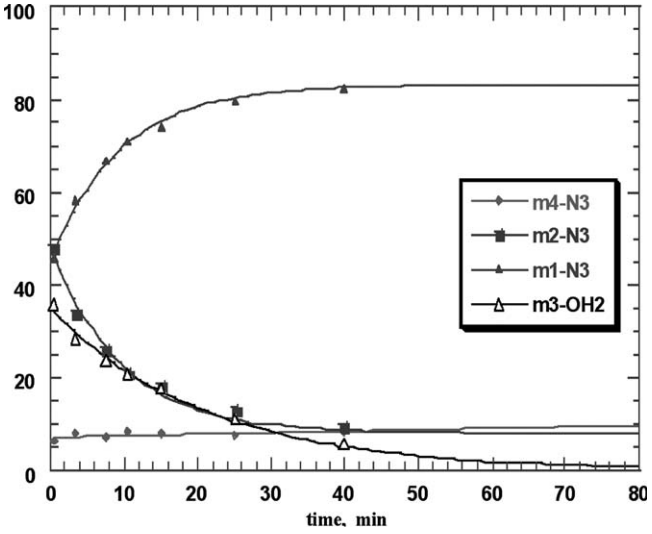

Fig. 10. Evolving $[Co(dien)(ampy)N_3]^{2+}$ product distributions for the m3-OH_2 reactant in 1.0 M NaN_3 at 20 °C (note that the reactant is actually the hydroxo complex, albeit the leaving group is water – see text). The vertical axis is % total complex.

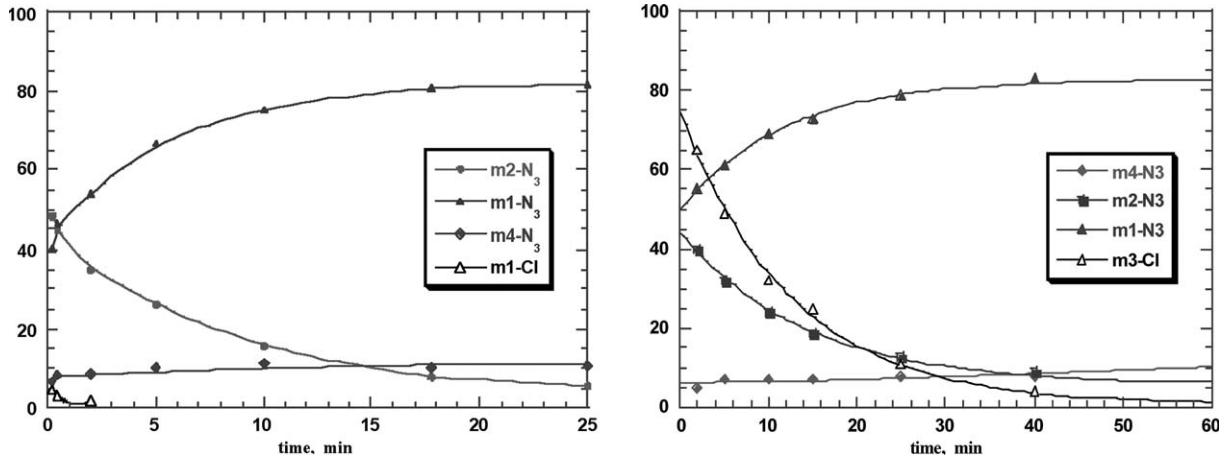

Fig. 9. Evolving $[Co(dien)(ampy)N_3]^{2+}$ product distributions for the m1-Cl (left) and m3-Cl (right) reactants in 1.0 M NaN_3 at 20 °C. The vertical axes are % total complex.

The reaction of the m2-aqua isomer in 3 M triflic acid was followed at two temperatures, and the clean formation of the m1 isomer was observed (Fig. 11). This reaction requires N-inversion which is suppressed in acid solution, but it is noted that the alternative process of ligand folding [4] leads to an apparently inverted N-centre (*endo* to *exo*) but a different *mer* product (m3) (Fig. 12). Also, the latter process is usually very very slow.

On repeating the experiments in 0.1 M triflic acid, a much faster (ca. 20-fold) m2 to m1 rearrangement was observed, and subsequent events, m1 to m4 and m3, with the m3 aqua ion predominant (80%) at equilibrium. We also observed the m4-aqua to m3-aqua isomerization in 3 M triflic acid, a slower reaction than the m2 to m1 process, but one that also involves N-inversion. In summary, it would seem that the m2-aqua isomer isomerises via base catalysed N-inversion, likely via the labile m2-OH complex.

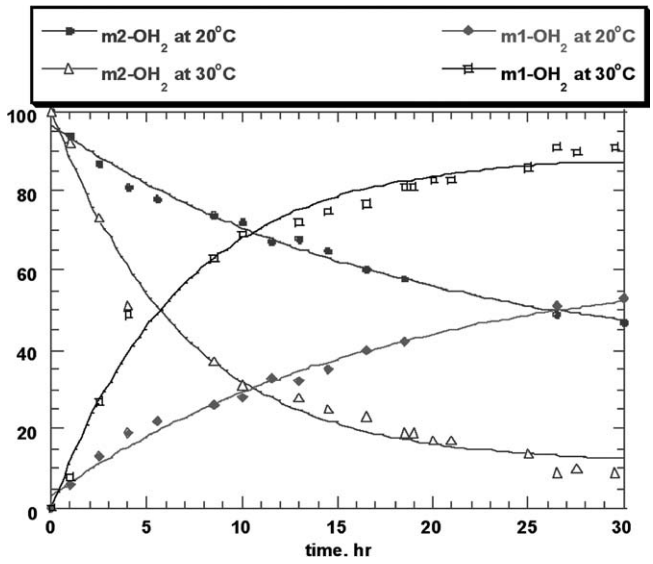

Fig. 11. Time dependence of the distribution of isomers derived from m2-$[Co(dien)(ampy)OH_2]^{3+}$ in 3 M aqueous triflic acid at 20 and 30 °C as a function of time. The vertical axis is % total Co.

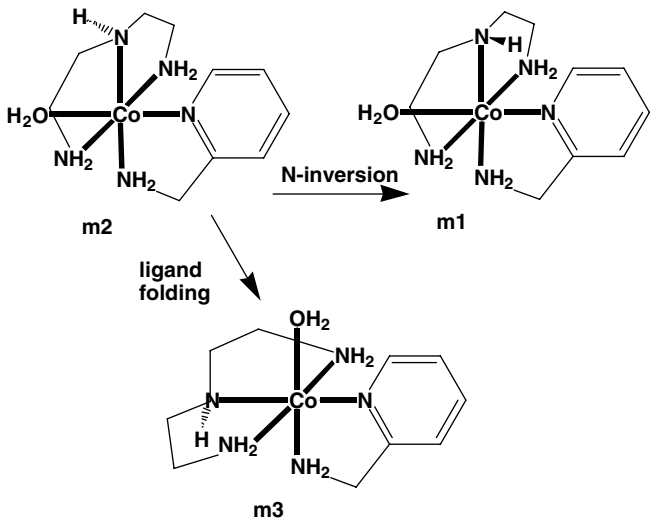

Fig. 12. Alternative reaction modes for m2-$[Co(dien)(ampy)OH_2]^{3+}$ in aqueous acid.

3.6. Rearrangement of the mer-hydroxo isomers and anti/syn isomerisation

There are two distinct processes – end to end (*cis*/*trans*) isomerisation, and *syn–anti* isomerisation. Either or both can occur via substitution, but *syn–anti* isomerisation can also occur by base catalysed N-inversion without ligand substitution. The following results for the *syn*/*anti* and *cis*/*trans* hydroxo ion distributions are averages over the four *mer* isomers, from two sources (four *mer* azido and four *mer* chloro ions).

Fig. 13 shows the time dependence of the $[Co(dien)(ibn)(OH)]^{2+}$ product distributions at about 20 °C. The distribution changes rapidly with time, and a common equilibrium distribution is attained which is quite different to the common kinetic distribution. These results also suggest that the isomerisations are not single phase exponential processes, but rather sequential processes, but the experimental error of ±5% for each isomer obscures the issue.

The corresponding distribution derived from the azido complexes as reactants is shown in Fig. 14. The middle stages are slightly different to those shown in Fig. 13 and probably reflect the greater error here because the primary hydrolysis and subsequent isomerisation steps are overlapped. The hydroxo complex distributions are normalized to 100%, and form of the decay curves for the azido ions are not shown.

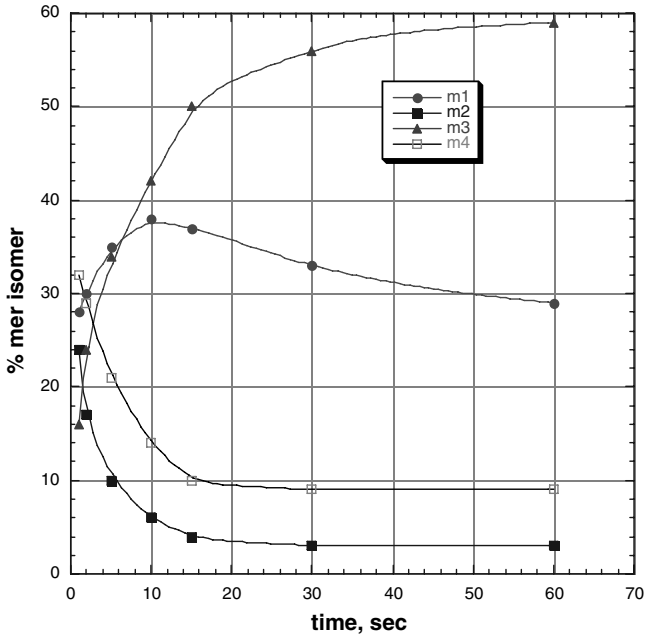

Fig. 13. Time-dependent *mer*-$[Co(dien)(ibn)OH]^{2+}$ distributions following the base hydrolysis of $[Co(dien)(ibn)Cl]^{2+}$; 0.5 M NaOH, ca. 20 °C.

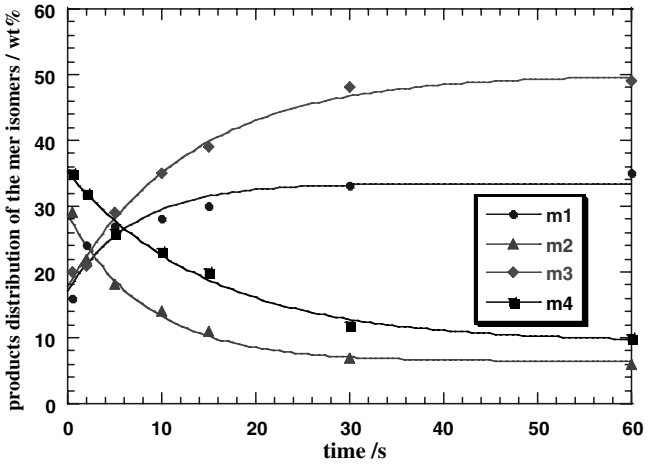

Fig. 14. The distribution of isomeric *mer*-hydroxo products for the base hydrolysis of the *mer*-$[Co(dien)(ibn)N_3]^{2+}$ isomers at ca. 20 °C.

The *anti*/*syn* isomer ratio for the $[Co(dien)(ibn)(OH)]^{2+}$ products increases smoothly with time (Fig. 15). The isomerization reactions derived from the azido substrates may be adjudged somewhat faster, but the initial and final values agree. The apparent rate difference probably reflects the lack of good temperature control for the different product distribution experiments; rates, however, were not the issue here.

The *cis*/*trans* isomer distributions as a function of time (Fig. 16) are less of an issue since the kinetic and equilibrium distributions are not greatly different.

Fig. 17 shows the initial (kinetic) product distribution derived from the m3-$[Co(dien)(ampy)Cl]^{2+}$ complex and how the $[Co(dien)(ampy)OH]^{2+}$ isomer distribution evolves with time. The *syn–mer–cis* (m2) isomer was never observed. The m1-OH isomer was the dominant initial product (76%), but the more stable m3-OH species became the major species in time, with 80% at equilibrium. Other experiments (Fig. 18) were carried out on the m3-OH complex, as reactant and under the same conditions, to ascertain the relative rates of subsequent epimerization from these curves it is clear that base hydrolysis of the chloro reactant is much faster than the subsequent isomerization of the hydroxo complexes, as found for the ibn system. Also, the rates of m1-OH/m3-OH equilibration for the two sets of experiments are the same, as they should be since the exponentials reflect the sum of the forward and reverse rate constants in both cases.

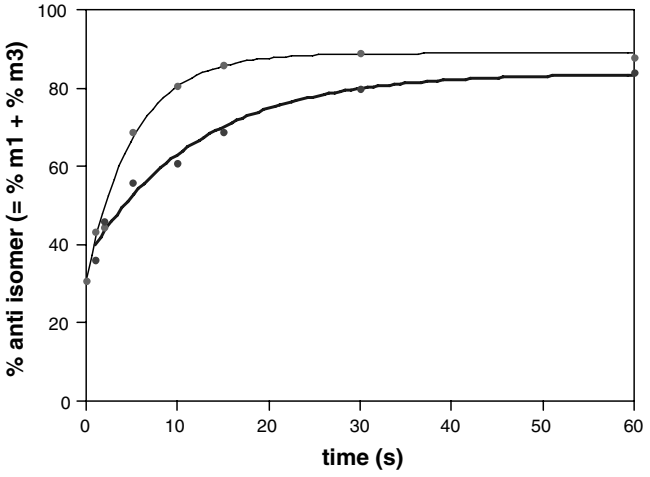

Fig. 15. *Anti*/*syn* product $[Co(dien)(ibn)OH]^{2+}$ distributions for the base hydrolysis of the *mer*-chloro (lower) and *mer*-azido ions (upper).

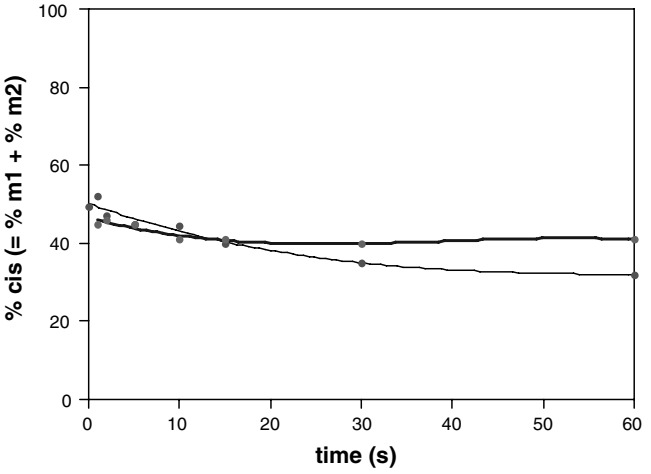

Fig. 16. *Cis*/*trans* product $[Co(dien)(ibn)OH]^{2+}$ distributions for the base hydrolysis of the *mer*-$[Co(dien)(ibn)Cl]^{2+}$ and *mer*-$[Co(dien)(ibn)N_3]^{2+}$ ions.

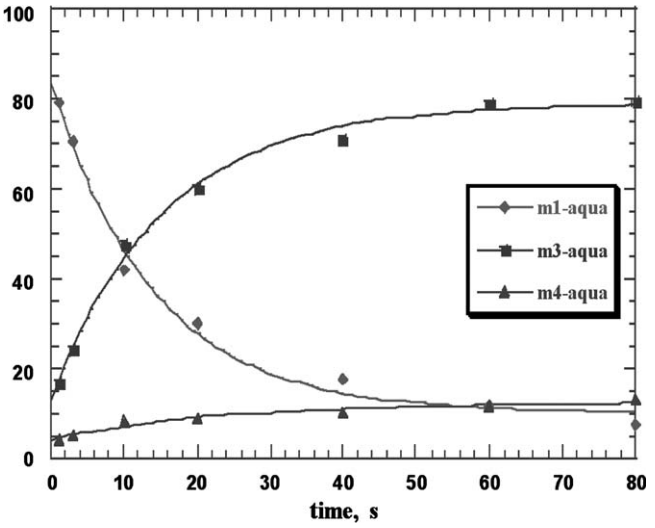

Fig. 17. Evolving $[Co(dien)(ampy)(OH)]^{2+}$ product distributions derived from the m3-chloro complex (0.5 M NaOD, 20 °C). The vertical axis is % total Co.

3.7. Formation and rearrangement of $[Co(dien)(ampy)OP(O)(OH)]^{+}$

In the earlier synthetic paper [2], we could prepare the elusive m1-Cl isomer via the equilibrated azido species, or better, via its phosphate complex. In $NaH_2PO_4/NaHPO_4$

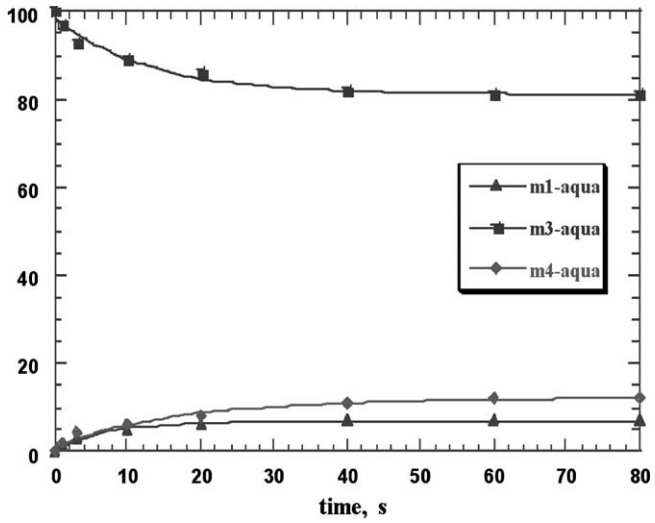

Fig. 18. Isomerisation of m3-[Co(dien)(ampy)OH]$^{2+}$ in 0.5 M NaOD at 20 °C. The vertical axis is % total Co.

buffers (pH 7.0–9.0), phosphate readily displaces Cl^- from any of the chloro complexes, and on standing there is almost a complete rearrangement to the m1 phosphato species, Table 7 (cf. 80% m3 in the absence of phosphate; Table 3).

Fig. 19 shows some idealised H-bonded structures for each of the four possible *mer* phosphate complexes. pH should be important in the H-bonding process in solution; at lower pH (3–4) phosphoric acid exists largely as $H_2PO_4^-$, whereas at higher pH (8–9) it is largely HPO_4^-. In addition, the acidity of the hydrogen phosphates will increase on O-coordination. Sites for Hbonding involve the terminal NH_2's of dien, common to all 4 *mer* isomers, the *sec*-NH centre, accessible only for the m2 and m4 isomers, and the terminal $-NH_2$ centre of the ampy ligand, accessible only for the m1 and m2 isomers. It would seem that the best prospects exist for the m1 isomer where the ligand is HPO_4^{2-} and two H-bonds can form. In $H_2PO_4^-$ media, more m4 is observed at equilibrium (50% m1, 20% m4), presumably because only one P–O oxygen is now accessible to H-bond to an amine, reducing the contribution from the H-bonded structure shown for the m1 isomer (Fig. 19).

Table 7
Product distribution for the reaction of *mer*-[Co(dien)(ampy)Cl]Cl_2 in NaH_2PO_4 (0.25 M)/NaOD(0.25 M)/D_2O buffer; 50 min at 20 °C

Phosphato isomer →	f1	f2	f3	m1	m2	m3	m4
m1-Cl				93		5	2
m2-Cl				94		5	1
m3-Cl				92		6	2
m4-Cl				90		6	4

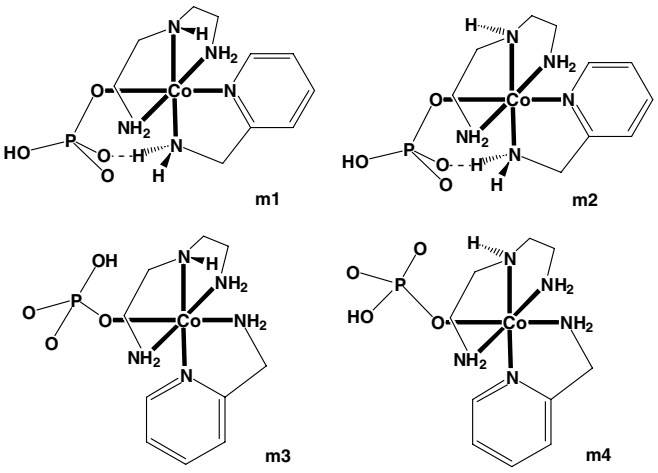

Fig. 19. Proposed H-bonded phosphate structures.

3.7.1. X-ray structure of m1-[Co(dien)(ampy)OP(OH)$_3$]$Cl_3 \cdot 2H_2O$

The complex crystallised from acid solution as the fully protonated form, confirmed by the X-ray structure which reveals three Cl^- anions per phosphato cation. As far as we are aware, this is the first reported structure for a metal complex of phosphoric acid.

The ORTEP diagram for the molecular cation is shown in Fig. 20. Selected bond lengths and angles are presented in Table 8. The dien rings adopt the chiral λλ or δδ conformations, and the crystal is a racemate. The bond lengths and angles are unremarkable. The P–O(1)Co length of 1.480(2) Å is appreciably shorter than the other P–OH bond lengths 1.529–1.558 Å. Although not symmetry

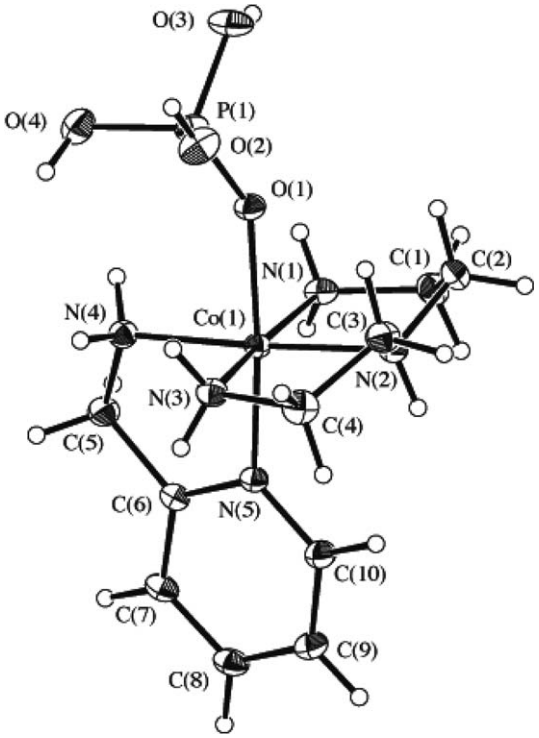

Fig. 20. ORTEP diagram for the molecular cation m1-[Co(dien)(ampy)-OP(OH)$_3$]$^{3+}$. Thermal displacement parameters are shown at the 20% level.

Table 8
Selected bond length (Å) and bond angle (°) data for m1-[Co(dien)-(ampy)$OP(OH)_3$]$Cl_3 \cdot 2H_2O$

Co(1)–O(1)	1.936(2)
Co(1)–N(1)	1.954(2)
Co(1)–N(2)	1.954(2)
Co(1)–N(3)	1.962(2)
Co(1)–N(4)	1.940(2)
Co(1)–N(5)	1.932(2)
P(1)–O(1)	1.480(2)
P(1)–O(2)	1.529(2)
P(1)–O(3)	1.526(2)
P(1)–O(4)	1.558(2)
O(2)–H(1)	0.77(4)
O(3)–H(2)	0.70(4)
O(4)–H(3)	0.82(3)
O(1)–Co(1)–N(1)	85.07(8)
O(1)–Co(1)–N(2)	87.81(8)
O(1)–Co(1)–N(3)	91.22(8)
O(1)–Co(1)–N(4)	89.34(9)
O(1)–Co(1)–N(5)	172.79(9)
N(1)–Co(1)–N(2)	86.2(1)
N(1)–Co(1)–N(3)	171.3(1)
N(1)–Co(1)–N(4)	93.21(9)
N(1)–Co(1)–N(5)	91.87(9)
N(2)–Co(1)–N(3)	85.8(1)
N(2)–Co(1)–N(4)	177.12(9)
N(2)–Co(1)–N(5)	98.52(9)
N(3)–Co(1)–N(4)	94.66(9)
N(3)–Co(1)–N(5)	92.69(9)
N(4)–Co(1)–N(5)	84.31(9)
O(1)–P(1)–O(2)	108.7(1)
O(1)–P(1)–O(3)	111.7(1)
O(1)–P(1)–O(4)	113.2(1)
O(2)–P(1)–O(3)	109.5(1)
O(2)–P(1)–O(4)	108.4(1)
O(3)–P(1)–O(4)	105.2(1)
Co(1)–O(1)–P(1)	147.7(1)
P(1)–O(2)–H(1)	115(3)
P(1)–O(3)–H(2)	120(3)
P(1)–O(4)–H(3)	113(3)

related, the two '*endo*' P–OH bond lengths are the same (1.526(2), 1.529(2) Å), and shorter than the '*exo*' P–OH (1.558(2) Å). Corresponding P–O bonds in the structures of H_3PO_4 and $H_3PO_4.0.5H_2O$ are 1.49 and 1.52 Å for P–O, 1.57 and 1.56 Å for P–OH. For a range of phosphates P–O is typically 1.51 Å and P–OH 1.55–1.58 Å [26].

3.8. Steric course of base hydrolysis of the $fac[Co(dien)(diamine)Cl]^{2+}$ isomers

The base hydrolysis of three facial $[Co(dien)(ibn)Cl]^{2+}$ isomers finished 'instantly' at high $[OD^-]$, and the product distributions were quite clearly dependent on the starting *fac* configuration (f1, f2 or f3), Table 3. There can be no common intermediate. The f2-Cl substrate yields f2 and f1 products, and no *mer*- or f3-OH isomers. The other two reactants, f1- and f3-Cl, yield two *fac* isomers along with a single *mer* product (Table 3). The product distributions for the f1 and f3 substrates are very similar in the sense that the 40:49:11 ratios are indistinguishable, save for the isomer designations, indicating that the *gem*-dimethyl groups in either of the two inequivalent positions on the diamine backbone have no real influence. Overall the results parallel those for other $[Co(dien)(diamine)Cl]^{2+}$ systems [14,23], where the data are less informative because the diamine (en, tn or dapo) is symmetrical.

These observations can be explained using sets of intermediates of the kind proposed for *mer* reactants, trigonal bipyramidal, but where the dien is facially arranged and the deprotonation site is presumed to occupy the trigonal plane. The facial isomers are asymmetric, and therefore all nine NH protons are inequivalent. The simplifying assumption is made that for any given facial isomer only one site is effectively deprotonated, and may be the same or different for each facial isomer.

For the f2 reactant, the results are accommodated by a single trigonal pyramidal (TBP) intermediate (Fig. 21).

The absence of f3 or any *mer* product can be understood in terms of the intermediate(s) that would be required (Fig. 22).

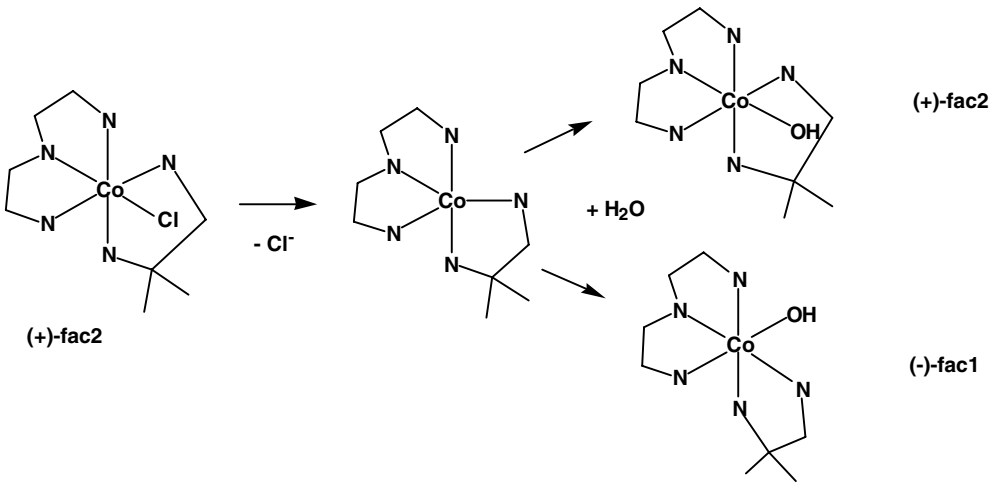

Fig. 21. The TBP derived from the f2 isomer of $[Co(dien)(ibn)Cl]^{2+}$, and the stereochemical consequences.

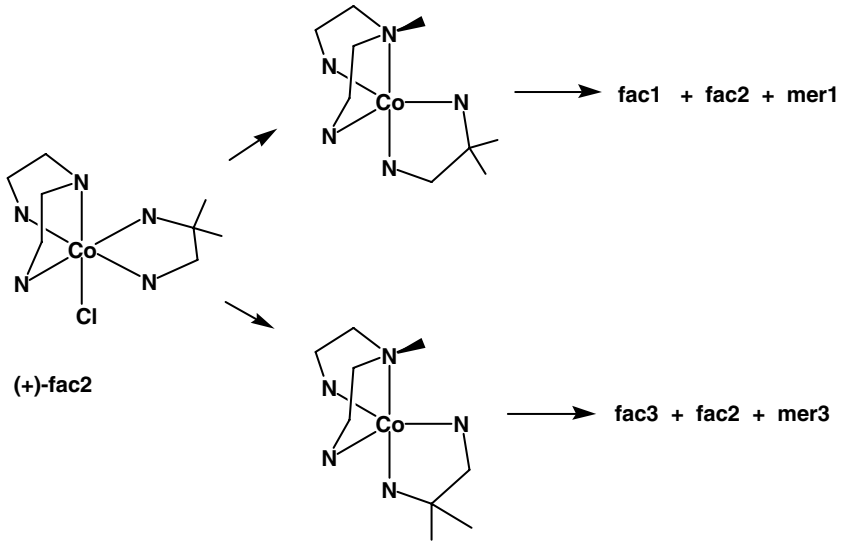

Fig. 22. The unfavoured TBP intermediates derived from the f2 isomer of $[Co(dien)(ibn)Cl]^{2+}$ by axial displacement of Cl^{-}.

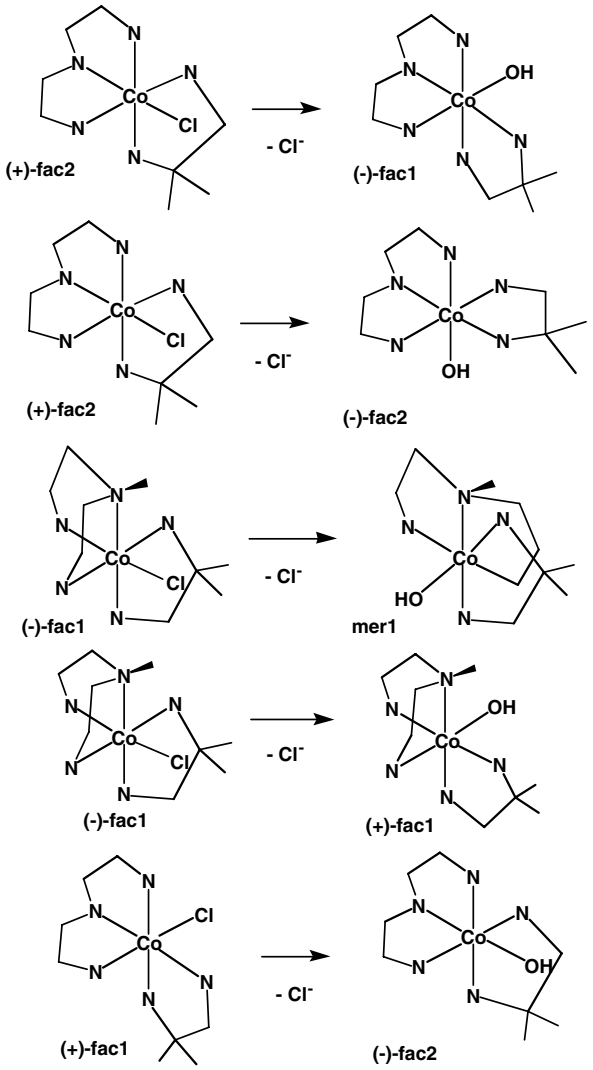

Fig. 23. Possible single-edge displacement processes. The set for the f3 reactant of $[Co(dien)(ibn)Cl]^{2+}$ (not shown) are generated by switching the *gem*-dimethyl substituents in the bidentate backbone of the f1 isomer and its product.

Considerable chelate arm movement is required to achieve either of the configurations shown, and it involves axial displacement of Cl^{-}. If the two intermediates shown were produced, they would appear in similar amounts, given that they differ only in the position of the *gem*-methyl groups, and thus would give rise to f3 and *mer* products.

The rearrangements of the *fac* isomers provide good examples of the edge displacement principle that is based on minimal rearrangement of the octahedron in any one substitution step [27,28]. Under this principle, and apart from the retentive processes that are always possible, only the direct isomerisations shown (Fig. 23) can occur; each process involves movement of a terminal chelate arm to the position occupied by the leaving group. The corresponding set for the f3 isomer (not shown) mirrors that for the f1, where inverted f3, (+)-f2, (−)-f2 and m3 are 'allowed' substitution products. Under these schemes,

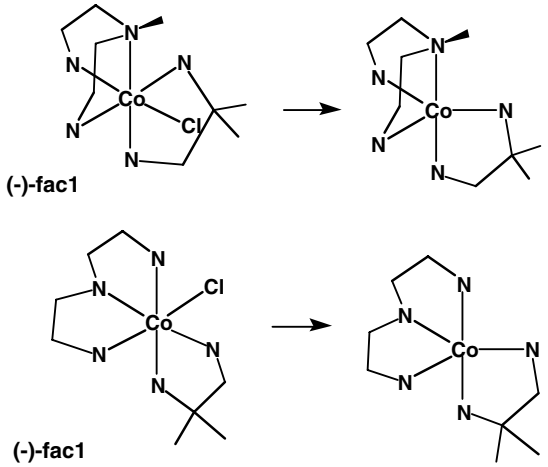

Fig. 24. Two feasible TBP intermediates derived from a f1-Cl reactant of $[Co(dien)(ibn)Cl]^{2+}$.

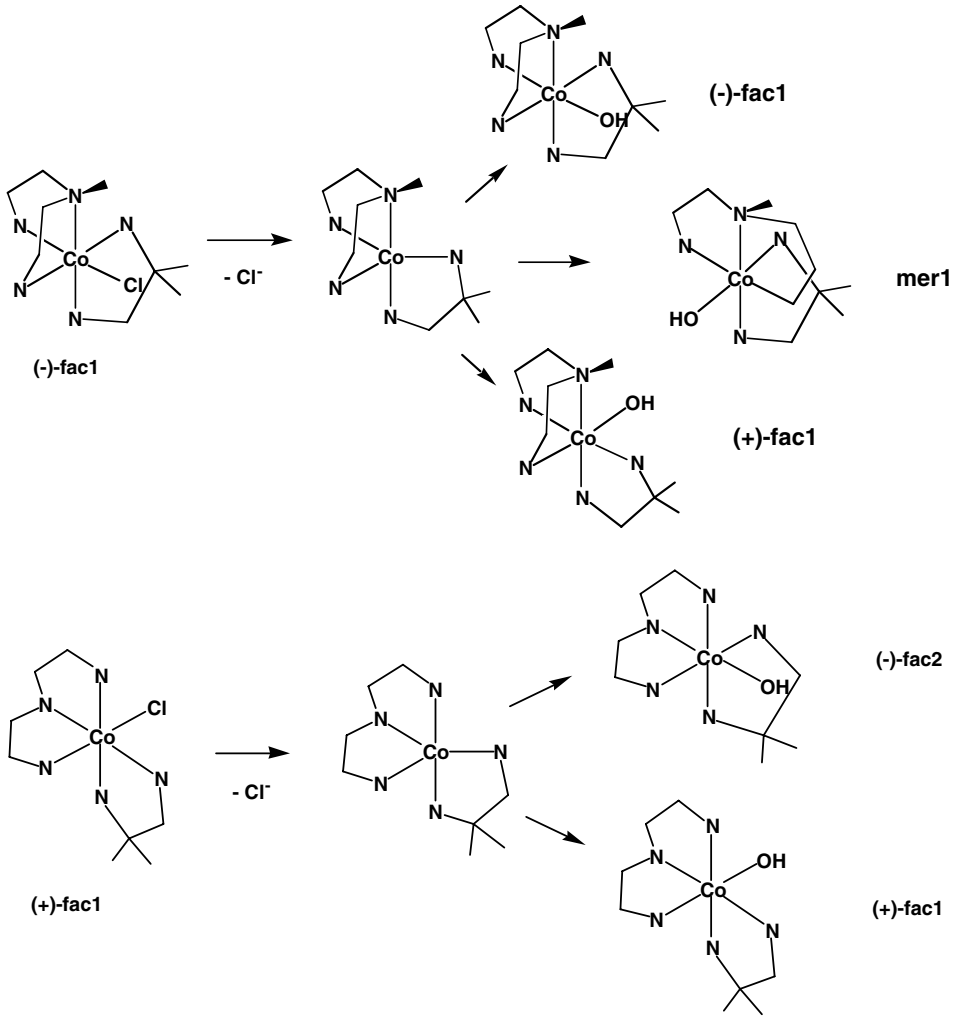

Fig. 25. The two TBP intermediates which account for the observed steric course of substitution of $[Co(dien)(ibn)Cl]^{2+}$.

direct interconversion of f1 and f3 is not allowed, and indeed is not observed.

Thus, far it has been assumed that water enters the intermediate along the trigonal plane. Microscopic reversibility *requires* water to be lost from the equatorial position for the reverse process regenerating the intermediate. It is therefore reasonable that equatorial loss of chloride is preferred, precluding the pathways above, and consistent with observation. Fig. 24 shows the same f1 reactant drawn in two perspectives to show how each TBP intermediate is formed by loss of equatorial Cl^- *cis* to deprotonated ibn.

These intermediates account for the observed product distributions (Fig. 25).

Some of the intermediates (Figs. 21 and 25) involve a five-membered chelate occupying the trigonal plane. In consideration of isomeric rearrangements in acid solution these are excluded [11,27,29], but in base hydrolysis they are clearly attainable (as demonstrated unequivocally for the *mer* substrates). Further, chiral forms are shown in all these figures, but all experiments were carried out on racemates, and clearly the mirror image structures are equally accessible.

The stereochemical results for the *fac*-ampy complexes are analogous to the ibn results, with some differences. The f1-Cl ion gives f1-, f2- and m1-OH products, but no f3 (nor any other *m*-OH isomer). There is much less m1 product than for the ibn analogue, and presumably the second intermediate with the pyridyl remote from the trigonal plane is favoured. Similarly, the f3-Cl isomer yields f3-OH and m3-OH, but unlike the ibn analogue, no f2-OH. The f2-Cl complex again gives just f2-OH and f1-OH, as in the ibn system, but now with considerably more of the latter. The reason for this is not obvious since the pyridyl is remote from the equatorial plane of the trigonal bipyramidal intermediate, and in any event, it parallels the symmetrical en system (Table 3).

4. Supporting information

Crystallographic data have been deposited with the Cambridge Crystallographic Data Centre, CCDC 274124.

Copies of this information may be obtained free of charge from The Director, CCDC, 12 Union Road, Cambridge CB2 1EZ, UK (fax: +44 1223 336 033; e-mail: deposit@ccdc.cam.ac.uk or www: http://www.ccdc.cam.ac.uk).

Acknowledgements

We are grateful to the Australian Research Council for financial support.

References

[1] T. Zhu, W.G. Jackson, Inorg. Chem. 42 (2003) 88.
[2] T. Zhu, W.G. Jackson, Inorg. Chim. Acta 343 (2003) 147.
[3] T. Zhu, Q.-J. Zhu, S.-F. Xie, W.G. Jackson, Z.-Y. Zhou, X.-G. Zhou, Polyhedron 22 (2003) 1603.
[4] T. Zhu, Z. Qian-jiang, X. Sai-fieng, W.G. Jackson, Z. Zhong-Yuan, Z. Xiang-Ge, J. Mol. Struct. 703 (2004) 83.
[5] W.G. Jackson, Inorg. React. Mech. (Abingdon, United Kingdom) 4 (2002) 1.
[6] W.G. Jackson, C.M. Begbie, M.L. Randall, Inorg. Chim. Acta 70 (1983) 7.
[7] J.M. Harrowfield, A.M. Sargeson, B. Singh, J.C. Sullivan, Inorg. Chem. 14 (1975) 2864.
[8] A.J. Dickie, D.C.R. Hockless, A.C. Willis, J.A. McKeon, W.G. Jackson, Inorg. Chem. 42 (2003) 3822.
[9] SIR-92 A. Altomare, M. Cascarano, C. Giacovazzo, A. Guagliardi, J. Appl. Crystallogr. 26 (1993) 343.
[10] teXsan, Single Crystal Structure Analysis Software, Version 1.7, Molecular Structure Corporation, MSC, 3200 Research Forest Drive, The Woodlands, TX 77381, USA, 1992–1997.
[11] W.G. Jackson, A.M. Sargeson, Inorg. Chem. 17 (1978) 1348.
[12] W.G. Jackson, J.M. Harrowfield, P.D. Vowles, Int. J. Chem. Kinet. 9 (1977) 535.
[13] W.G. Jackson, A.M. Sargeson, Org. Chem. 42 (1980) 273.
[14] W.G. Jackson, P.B. Spencer, R.J. Walsh, Inorg. Chim. Acta 284 (1999) 37.
[15] R.W. Hay, D.A. House, Inorg. Chim. Acta 19 (1976) 23.
[16] T.K. Huan, J.N. Mulvihill, A.R. Gainsford, D.A. House, Inorg. Chim. Acta 12 (1973) 517.
[17] L.S. Dong, D.A. House, Inorg. Chim. Acta 19 (1976) 23.
[18] D.A. House, A.R. Gainsford, J.W. Blunt, Inorg. Chim. Acta 57 (1982) 141.
[19] M.L. TobeAdvances in Inorganic and Bioinorganic Mechanisms, vol. 2, Academic Press, New York, 1983, p. 1.
[20] T.K. Huan, J.N. Mulvihill, A.R. Gainsford, D.A. House, Inorg. Chem. 12 (1973) 1517.
[21] R.W. Hay, K.B. Nolan, J. Inorg. Nucl. Chem. 38 (1976) 2118.
[22] F.A. Ha, D.A. House, Inorg. Chim. Acta 38 (1980) 167.
[23] P. Comba, W.G. Jackson, W. Marty, L. Zipper, Helv. Chim. Acta 75 (1992) 1147.
[24] P. Comba, W.G. Jackson, W. Marty, L. Zipper, Helv. Chim. Acta 75 (1992) 1172.
[25] D.G. Gaswick, J.A. McKeon, W.G. Jackson, results reported in Ref. [5].
[26] A.F. Wells, Structural Inorganic Chemistry, Clarendon Press, Oxford, 1984.
[27] F. Basolo, E.G. Pearson, Mechanisms of Inorganic Reactions, second ed., Wiley, New York, 1967.
[28] D.D. Brown, C.K. Ingold, R.S. Nyholm, J. Chem. Soc. (1953) 2673.
[29] W.G. Jackson, in: I. Bernal (Ed.), The Stereochemistry of the Bailar Inversion and Related Substitution Processes, vol. 1, Elsevier, Amsterdam, 1986, p. 255.